Dalton Transactions

Distinguishing deposition, corrosion, and stripping of transient heterogeneous materials during molecular electrocatalysis

Journal:	*Dalton Transactions*
Manuscript ID	DT-ART-02-2019-000584.R1
Article Type:	Paper
Date Submitted by the Author:	14-Mar-2019
Complete List of Authors:	Sconyers, David; University of Kansas, Department of Chemistry Blakemore, James; University of Kansas, Department of Chemistry

Journal Name

ARTICLE

Distinguishing deposition, corrosion, and stripping of transient heterogeneous materials during molecular electrocatalysis

Received 00th January 20xx,
Accepted 00th January 20xx

DOI: 10.1039/x0xx00000x

www.rsc.org/

*David J. Sconyers[a] and James D. Blakemore[a]**

Understanding the behavior of molecular hydrogen-evolving electrocatalysts is often challenging, because secondary heterogeneous materials can form during reductive electrode polarization and contribute to catalysis. Here, we use an electrochemical quartz crystal microbalance to interrogate secondary heterogeneous materials formed *in situ* during hydrogen generation with the proton- and difluoroboryl-bridged dimethylglyoxime cobalt catalysts in acetonitrile electrolyte. Detrimental protonation reactions of the molecular precatalysts lead to formation of the transient heterogeneous materials, and the structure of the molecular cobaloxime precursors affects the potential dependence and kinetics of deposition and loss of heterogeneous material from the electrode surface. The strength of the acid in the electrolyte (needed as the proton source for H_2 generation) also contributes to the stability and corrosion rate of the heterogeneous materials, as revealed in multistep polarization studies. Overall, these results support involvement of an interplay of electrodeposition, proton-driven (chemical) corrosion, and anodic (electrochemical) stripping in influencing the catalytic activity and the behavior of transient heterogeneous materials that may be generated during catalysis.

1. Introduction

Electrochemical hydrogen evolution is often discussed in the context of clean energy storage, as H_2 derived from water splitting represents a possible clean fuel. In electrochemical generation of H_2 from water, protons and electrons (reducing equivalents) must be coupled together by a catalyst:

$$2H^+ + 2e^- \rightarrow H_2$$

Many catalysts have been studied for proton reduction, including metal surfaces,[1] colloids,[2,3] nanoparticles,[4,5] organic compounds,[6,7] and metal complexes. Molecular catalysts have been especially useful for understanding the reaction mechanisms that enable H_2 generation, as they can be readily studied in homogeneous solution.[8,9] Indeed, a variety of spectroscopic techniques can be applied to reveal the individual elementary steps involved in H_2 generation, as well as any speciation processes that limit availability of the active catalyst in solution. Techniques in molecular electrochemistry are especially useful for study of H_2 generation, as they can be used to understand the steps involved in catalysis.[10,11] Typically, a precatalyst is envisioned to undergo reduction at the electrode, react with protons available in solution, form one or more transient intermediates, and eventually evolve product H_2.

However, understanding the mechanism of molecular catalysis is often challenging in electrochemical experiments. The electrochemical data alone offer little insight into the structure of the intermediates involved in catalysis.[12] Additionally, the conditions required for hydrogen evolution are often harsh, involving large excesses of acid (necessary as the source of protons) as well as strongly reducing potentials. These factors can result in unanticipated reactivity or lead to generation of unanticipated secondary species from the molecular precatalysts. Moreover, as the volume of the reaction-diffusion layer at the electrode is often small in comparison with the total cell volume, the amount of any active intermediates present at a given moment is typically a tiny fraction of the total catalyst loading.[13,14] Chemically- or electrochemically-induced speciation is often challenging to observe, but influences the effectiveness of a given molecular catalyst.

The formation of secondary heterogeneous species in electrocatalytic studies is problematic, as such material can remain immobilized on the electrode surface over long times and contribute to the observed catalysis.[15] Such solids are difficult to detect by spectroscopic measurements made on working solutions, as the amounts of material involved are small. Although *ex situ* methods (e.g., microscopy, photoelectron spectroscopy) can be used to interrogate electrode surfaces for the presence of secondary materials, these measurements can be complicated by sample handling that leads to loss of material before completion of the analysis.[16,17,18] *In situ* spectroscopic and spectroelectrochemical methods avoid this challenge, and can provide rich details on the behavior of electrocatalytic systems.[19]

[a] *Department of Chemistry, University of Kansas, 1567 Irving Hill Road, Lawrence, Kansas 66045, USA*

Electronic Supplementary Information (ESI) available: [details of any supplementary information available should be included here]. See DOI: 10.1039/x0xx00000x

Cobaloximes are among the most celebrated catalysts for hydrogen evolution.[20,21] Originally developed as model compounds for vitamin B12,[22,23,24] they are built on a macrocyclic ligand framework formed by chelation and deprotonation of two dimethylglyoxime units. The parent cobalt complex ($Co^{II}(dmgH)_2$, **1**) thus features two glyoximato ligands bridged by protons. Drago[25] and Busch[26] showed that the bridging protons can be replaced by difluoroboryl bridges, providing ready access to the popular derivative $Co^{II}(dmgBF_2)_2$ (**2**). As these compounds are straightforward to prepare, derivatives of these catalysts have been incorporated into a variety of systems for hydrogen evolution.[27,28,29,30,31]

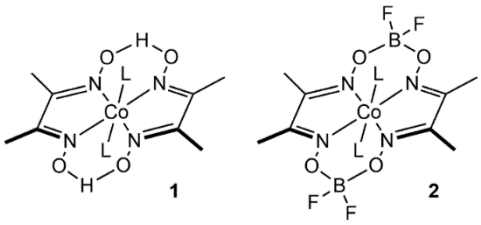

Chart 1. Structures of the cobalt complexes discussed in this study.

Building on the early work, cobaloximes have been widely studied, especially with regard to their catalytic mechanism.[32,33,34] Computational studies from Muckerman and Fujita[35] and experimental work from Winkler, Gray, and co-workers[36] support involvement of a cobalt(II) hydride in molecular catalysis with **2**. Investigations centered on the participation of cobalt hydrides in H_2 evolution with **2** remains a topic of high interest.[37,38,39]

Ligand exchange is an important factor that influences catalysis with H-bridged cobaloximes, like **1**.[40] Specifically, rapid ligand exchange has been observed under turnover conditions, suggesting that **1** is dynamic in the presence of acid and/or reductants. Decomposition of **2** in the presence of a strong organic acid has also been measured spectroscopically in the absence of a reducing potential.[41] On the other hand, formation of cobalt nanoparticles on an electrode under acidic aqueous conditions was observed using **2** as a molecular precursor.[42] Similar observations have also been made for a related diimine-dioxime catalyst.[43,44] Hydrogenation and decomposition following reduction in the presence of strong acid has also been measured for cobaloximes.[45,46]

We recently reported the use of an electrochemical quartz crystal microbalance (EQCM) to interrogate the speciation of **2** under acidic conditions in acetonitrile (MeCN).[47] This approach provides new insight for studies of catalyst speciation at electrode surfaces, because the EQCM provides a direct readout of the mass of the working electrode during electrochemical potential cycling.[48] Based on our EQCM studies and related chemical experiments, we have proposed pathways for the decomposition of **1** and **2** that can give rise to heterogeneous, catalytically active material. We also directly observed corrosion of the electrodeposited material arising from **2**, demonstrating that *ex situ* analysis of the electrode surface under these conditions would be insufficient for detection of heterogeneous material.

In this manuscript, we report EQCM studies comparing **1** and **2** during electrochemical cycling, and explore differences in their interfacial behavior as a function of the strength of added acid. Nuclear magnetic resonance and infrared spectroscopic data provide evidence for precatalyst speciation under acidic conditions, and support the general observation that ligand structure plays an important role in influencing the accessible speciation modes. With the EQCM, we investigate the electrodeposition behavior that results from the acid-promoted speciation, and have identified both corrosion and anodic stripping processes for the heterogeneous materials formed *in situ*. Overall, our findings support that an interplay between the deposition, corrosion, and stripping behaviors influences the behavior of these systems.

2. Results and Discussion

Synthesis and speciation of molecular precatalysts under acidic conditions

The glyoxime **1** was prepared according to Schrauzer's procedure,[49] by combining two equiv. of dimethylglyoxime ($dmgH_2$) with a single equiv. of cobalt(II) acetate tetrahydrate in MeCN. Coordination of the glyoxime ligands generates the product **1**, as well as two equiv. of acetic acid (detectable by this acid's distinctive odor) that are washed away during purification of the complex. To prepare **2**, we modified the procedure from Drago[25] in which installation of the bridging [BF_2] moieties is achieved through treatment of **1** with a large excess of $BF_3{\cdot}Et_2O$. We initially attempted to prepare **2** with MeCN as the solvent, as both **1** and $BF_3{\cdot}Et_2O$ are fully soluble. However, these conditions result in poor yields of **2** and generation of a mixture of products. Specifically, electrochemical studies suggest contamination of the desired **2** with $[Co(MeCN)_6]^{2+}$ (See ESI, Figure S12).

We have found that use of Et_2O as the solvent for installation of the [BF_2] bridges provides clean **2**, despite the fact that neither **1** nor **2** are soluble under these conditions. However, two stoichiometric equiv. of hydrogen fluoride (HF) are liberated upon formation of **2**. This mirrors the synthesis of **1**, in which acetic acid is generated *in situ* and then washed away; HF, on the other hand, appears to react with **2** and drive decomposition.[50] We postulate that the increased solubilities of the starting material **1** and the product **2** in MeCN (vs. Et_2O) are sufficient to facilitate interaction with the evolving HF, leading to decomposition and formation of $[Co(MeCN)_6]^{2+}$. Thus, when **2** forms in Et_2O, it immediately precipitates—a reaction that limits exposure to the acid present, thus preventing decomposition.

These new observations are in agreement with our prior report,[47] in which we described evidence for $[Co(MeCN)_6]^{2+}$ generation upon treatment of **2** with 2 equiv. of the strong acid protonated dimethylformamide ($[DMFH]^+$, p*K*a = 6.1 in MeCN).[51] Along with the formation of $[Co(MeCN)_6]^{2+}$, spectroscopic evidence supports demetallation of the

macrocyclic ligand framework of **2** upon treatment with $[DMFH]^+$. Specifically, a new feature is observed by IR spectroscopy at 614 cm^{-1}, attributable to protonated imines.[52] In accord with this assignment, vibrations attributable to O–H groups, which could be putatively formed by protonolysis of the O–B–O units in **2**, are not observed. As ^{11}B and ^{19}F NMR indicate that the material produced is diamagnetic and highly symmetric (point group C_{2v}), we have concluded that the product is $(dmgBF_2)_2H_2$ (**4**; see Scheme 1), a protonated metal-free macrocycle. $[Co(MeCN)_6]^{2+}$ is the co-generated product that arises from formation of free $[Co^{2+}]$ in MeCN.[53]

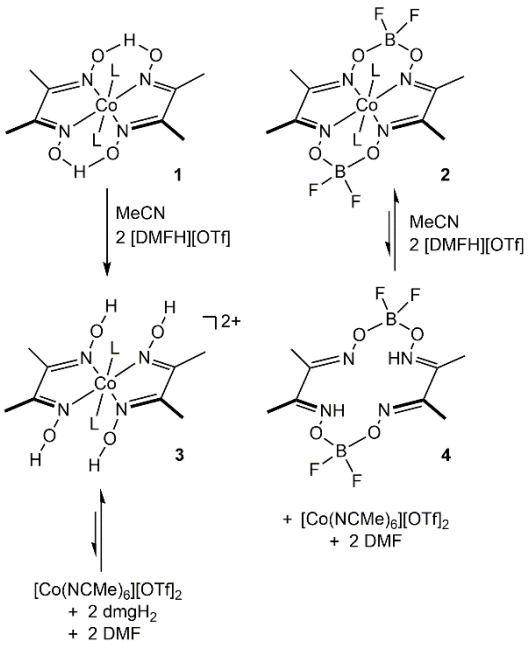

Scheme 1. Reaction scheme illustrating the proposed decomposition routes of **1** and **2** upon addition of strong acid.

Extending these chemical studies to **1**, infrared spectra collected on a solution of as-synthesized **1** in THF reveal a strong vibration at 1555 cm^{-1} that is assigned to the C–N stretch of the glyoxime ligand.[54] Following addition of two equivalents of $[DMFH]^+$ to **1**, a new stretch appears at 1654 cm^{-1} with concomitant attenuation of the original C–N stretch at 1555 cm^{-1} (see Figure 1, panel a). The new signal at 1654 cm^{-1} does not correspond to free ligand ($dmgH_2$, C–N stretch at 1443 cm^{-1}) or any signals that arise from mixing $dmgH_2$ and $[DMFH]^+$ (see ESI, Figures S1-S4 for spectra). However, a new, broad absorption is observed at 3300 cm^{-1} upon treatment of **1** with 2 equiv. of $[DMFH]^+$; this absorption resembles the broad O–H stretching vibration of the free ligand $dmgH_2$ (see Figure 1, panel b), suggesting protonation of **1** results in formation of O–H moieties. Together, these results suggest that a new cobalt-containing species could be the product of protonation of **1** with $[DMFH]^+$.

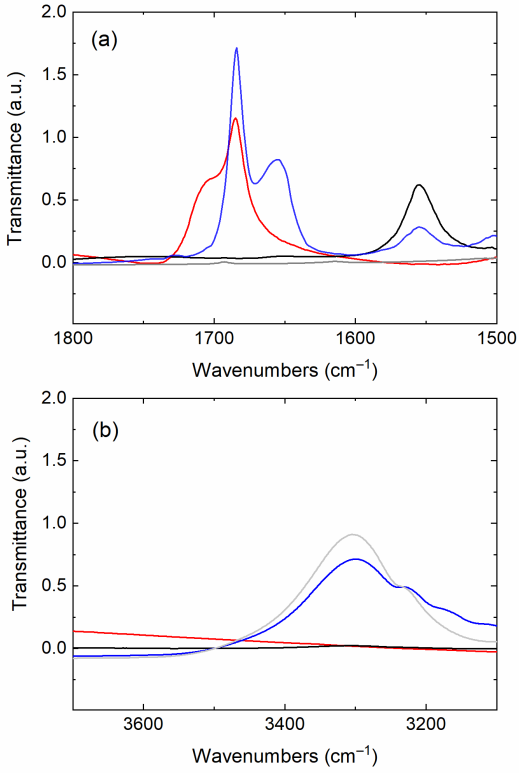

Figure 1. IR spectrum of a solution containing **1** (black), **1** treated with 2 equiv. $[DMFH]^+[OTf]^-$ (blue), $[DMFH]^+[OTf]^-$ alone (red) and $dmgH_2$ (gray). (a) depicts the region of the C-N stretching vibration, (b) depicts the region of the spectrum containing the O-H stretching vibration.

UV-visible absorption spectroscopy also provides support for generation of a unique cobalt complex under these conditions. The absorption spectrum of **1** exhibits three distinctive bands with λ_{max} values of 257, 300, and 425 nm in MeCN (see ESI, Figure S6). Upon addition of $[DMFH]^+$, these bands give way to a new, strongly absorbing feature at λ_{max} = 320 nm (see ESI, Figure S8). Notably, the solvento complex $[Co(MeCN)_6]^{2+}$ displays a broader and weaker absorption over the same wavelength range (approximately 440–550 nm; see ESI, Figure S7). As free $dmgH_2$ does not display visible absorptions, we conclude that there is a unique product formed upon addition of $[DMFH]^+$ to **1**, consistent with the formulation $Co(dmgH_2)_2^{2+}$ (**3**; see Scheme 1).

For structural insight into this system, we turned to ^1H NMR spectroscopy. The ^1H NMR spectrum of free $dmgH_2$ in CD_3CN reveals a singlet corresponding to the two equivalent methyl groups at 1.95 ppm, overlapping with the CD_3CN solvent residual signal, as well as a second singlet at 9.08 ppm corresponding to the oxime protons of the free ligand (see ESI, Figures S9-S11 for all NMR spectra discussed here). Conversely, there is no corresponding methyl signal for isolated **1**, in accord with the paramagnetism of the cobalt(II) center. However, solutions of **1** reliably display a broad resonance centered at 14.7 ppm that may be ascribed to the bridging protons of the macrocyclic ligand framework. Upon treatment of **1** with three equivalents of $[DMFH]^+$, the broad singlet shifts upfield to 9.08 ppm and sharpens noticeably. As the position of this signal is similar to that of the free $dmgH_2$ oxime protons

at 9.1 ppm, the NMR data suggest that the bound glyoximato ligands have become protonated under these conditions. Consistent with the IR data, no other upfield resonances are detected following addition of acid, supporting the conclusion that virtually no $dmgH_2$ ligand is released upon protonation.

Based on these studies, we propose that the primary decomposition product resulting from treatment of **1** with strong acid is not free $dmgH_2$ ligand, but rather a compound (**3**) that contains two bidentate dimethylglyoxime ligands (2x coordinated $dmgH_2$) (see Scheme 1). The ligands remain bound to the cobalt(II) center but have been protonated at the oxygen position—this breaks the two low-barrier hydrogen bonds between oxygen sites[55] and pairs protons with all the oximato moieties in the compound. Such protonated structures have been previously hypothesized[34,56] to be involved in molecular catalysis, but have been anticipated to be difficult to detect considering the propensity of cobalt(II) centers to undergo ligand exchange. Indeed, such ligand exchange was observed by Eisenberg in studies of **1** under acidic conditions.[40]

The unique features of the macrocyclic ligands in complexes **1** and **2** thus give rise to a unique acidic speciation pathway in each case. **1** features a glyoximato framework that can be readily protonated at the oxime oxygens, resulting in the elimination of the bridging hydrogen-bonding interactions and generating protonated cobalt complex **3**. This reaction apparently does not disturb the bidentate L_2-type chelating $dmgH_2$ ligands, which are observed only as bound to the cobalt center. However, these ligands seem poised to readily exchange with other coordinating groups or solvent. In contrast, acid-driven decomposition of **2** results in generation of a protonated macrocyclic compound, $(dmgBF_2)_2H_2$ (**4**), that cannot readily bind the free cobalt(II) metal center, resulting in ejection of $[Co(MeCN)_6]^{2+}$ into solution.[47] As the macrocycle is not broken, we have inferred that the geometry of the metal-binding site is blocked by the protons delivered from $[DMFH]^+$. However, depletion of acid from the environment containing **4** (for example, by reduction of protons to form H_2) would restore a strongly chelating L_2X_2-type framework with strong propensity to bind cobalt(II) ions.

As an aside, the unique decomposition pathways operative in the two cases discussed here are visible to the naked eye. Due to the large difference between the apparent molar absorptivity (ε) of **3** (≥5870 M^{-1} cm^{-1} at 320 nm) and the known smaller ε of $[Co(MeCN)_6]^{2+}$ (30 M^{-1} cm^{-1} at 480 nm) produced from **2**, visual inspection suggests that the decomposition of **1** and **2** lead to very different products. Addition of acid to **1** results in a color change, while addition of acid to **2** results in nearly complete bleach of all solution color. However, species arising from minor solvation equilibria with **3**—namely $[Co(MeCN)_6]^{2+}$ or a solvento species chelated by only a single $dmgH_2$ ligand—are unlikely to be observable by the spectroscopies used here. Thus, we additionally propose that the labile cobalt(II) center in **3** could rapidly exchange bidentate $dmgH_2$ ligands in the presence of excess coordinating solvents, like MeCN. This is consistent with prior work on ligand exchange under acidic conditions,[40] and is in accord with electrochemical results (*vide infra*) that support a role for $[Co(MeCN)_6]^{2+}$ in the behavior encountered for solutions containing **3**.

Voltammetry of precatalyst 1

In the absence of acid, cyclic voltammograms of **1** display a quasi-reversible one-electron reduction at ca. –1.5 V versus the ferrocenium/ferrocene couple (denoted hereafter as $Fc^{+/0}$) with ΔE_p = 80 mV at 100 mV/s (where ΔE_p is peak-to-peak separation) (see Figure 2, gray line). This process can be assigned as a formally cobalt(II/I) reduction. In addition, there is a broader couple with a midpoint potential near –0.3 V vs. $Fc^{+/0}$, assigned to cobalt(III/II) interconversion. In comparison with **2**, we have observed that the cobalt(II/I) couple for **1** is shifted 610 mV more negative than that observed with **2**, in agreement with prior work.[32,47] Additionally, **2** does not display a cobalt(III/II) couple within the voltage range explored here, an effect resulting from the electron-withdrawing nature of the bridging $[BF_2]$ groups.

Addition of 3 equiv. of $[DMFH]^+[OTf]^-$ to this solution containing **1** results in the appearance of a new irreversible reduction process at –1.2 V. This can be assigned as a pseudocatalytic response involving hydrogen generation (see Figure 2, black line). Scanning more negative, the initially present quasi-reversible cobalt(II/I) couple near –1.5 V is still observed. On the other hand, the cobalt(III/II) couple of **1** is severely attenuated upon addition of acid. Specifically, on an initial cathodic sweep that begins near 0 V, there is insignificant reductive current corresponding to generation of cobalt(II). Consistent with our chemical studies with acid, the electrochemical data confirms that **1** has been consumed upon acid addition, leading to generation of **3**, which does not undergo oxidation in this potential range. However, upon scanning through the catalytic response near –1.2 V in this quiescent solution (with concomitant consumption of acid, as implicated by the peaking pseudocatalytic process), **1** appears to be reformed in part, as we observe the corresponding cobalt(II/I) reduction for **1** near –1.5 V. This model is further supported by observation of the cobalt(II) oxidation wave near –0.15 V, corresponding to the presence of a population of **1** near the electrode after the cathodic potential excursion but not before.

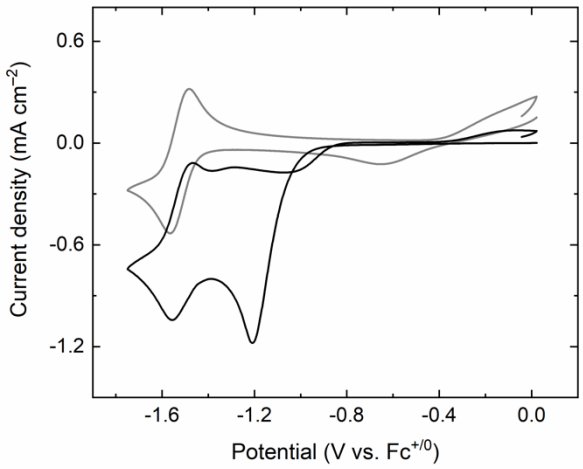

Figure 2. Cyclic voltammogram of the proton-bridged cobaloxime complex **1** with and without added acid. Gray: 2 mM **1**. Black: 2 mM **1** + 3 equiv. $[DMFH]^+[OTf]^-$. (MeCN, 0.1 M $[^nBu_4N][PF_6]$. Working electrode: highly oriented pyrolytic graphite. Scan rate 100 mV/s.)

In addition, voltammograms of **1** with 3 equiv. of $[DMFH]^+[OTf]^-$ acid present (Figure 2) display "crossing behavior" near –1.2 V. The "turn off" of catalysis near –1.2 V occurs at a more positive potential on the anodic sweep versus the cathodic sweep. Thus, the electrode is apparently more active for hydrogen generation following cathodic excursion than before, suggesting formation of a quantity of a catalytically active species by reduction. This observation casts doubt on the nature of molecular catalysis in the response at –1.2 V, and encourages use of the EQCM to obtain more information on the interfacial speciation of **1** under these conditions (*vide infra*).

EQCM studies of precatalysts 1 and 2

EQCM relies on the converse piezoelectric effect to enable monitoring of the mass of a working electrode in real-time during electrochemical experiments.[57] In the experiments described here, AT-cut quartz crystals serve as the piezoelectric component; the crystals are sputtered with gold, the conducting material that serves as the working electrode (electroactive area: 0.205 cm^2, total area ca. 1.33 cm^2). Each crystal has an intrinsic resonant frequency, vibrating when a driving alternating current is applied. The vibrational frequency is perturbed by mass changes at the surface (adsorption, electrodeposition, formation of insoluble materials, etc.), and the Sauerbrey equation relates the readily measured frequency change to apparent changes in mass.[58] We have previously leveraged the sensitivity of this technique, and can routinely measure mass changes on the order of ±5 ng (± 5 Hz).[47]

The electrochemical response of **1** at a gold working electrode closely resembles that observed on carbon. In the absence of added acid, the cobalt(II/I) couple is observed as a quasi-reversible wave at –1.5 V vs $Fc^{+/0}$ (ΔE_p = 170 mV) (Figure 3, black line). The cobalt(III/II) couple is also observed as on carbon. The gravimetric data (Figure 3, blue line) from simultaneous EQCM monitoring during voltammetry show no appreciable mass changes taking place at the electrode surface during voltammetry. Thus, on a sweep between 0 V and –1.7 V, passing through both the Co(III/II) and Co(II/I) couples, the electrolyte solution containing **1** remains homogeneous.

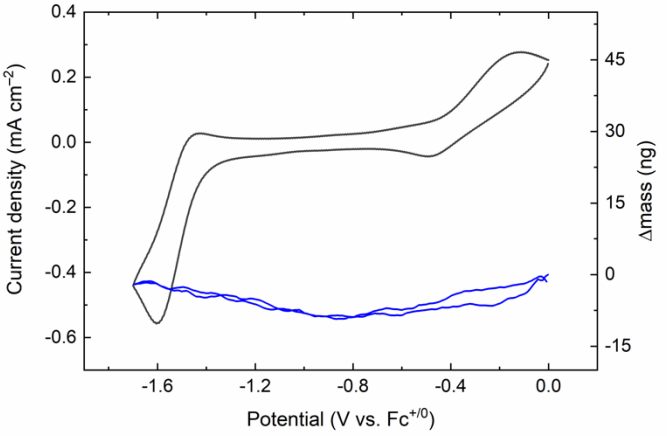

Figure 3. Electrochemical studies on **1** using the EQCM. 2 mM solution of **1**. Black: Current data, Blue: Mass data. (MeCN, 0.1 M $[^nBu_4N][PF_6]$. Working electrode: gold-coated quartz disk. Scan rate 100 mV/s.)

The voltammetric profile of a solution containing **1** plus 3 equiv. of $[DMFH]^+[OTf]^-$ is distinctive from the case without acid, in line with observations made in experiments carried out with carbon electrodes (Figure 4, panel a, black line). As before, a new reductive wave consistent with proton reduction catalysis appears with an onset potential near –1.0 V. The cobalt(II/I) couple centered at –1.5 V (ΔE_p = 170 mV) resembles that of the complex in the absence of acid, replicating the data obtained on carbon and implying consumption of acid during catalytic H_2 generation. Minor reductive features at –0.5 and –0.8 V are associated with the gold surface in acid, and thus do not involve **1** (see ESI, Figure S13). On the other hand, the wave associated with oxidation of **1** from Co(II) to Co(III) has a distorted appearance versus the case without acid, implicating formation of a new species undergoing oxidation at –0.4 V.

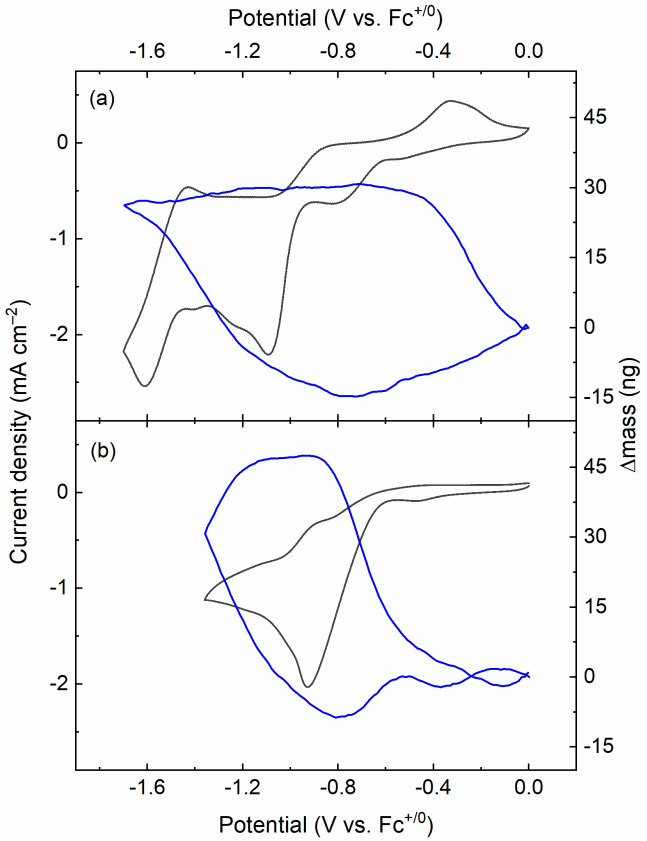

Figure 4. Electrochemical studies on **1** and **2** using the EQCM. (a) 2 mM solution of **1** treated with 3 equiv. $[DMFH]^+[OTf]^-$. Black: Current data, Blue: Mass data. (b) 2 mM solution of **2** treated with 3 equiv. [DMFH]+[OTf]–. Black: Current data, Blue: Mass data. (MeCN, 0.1 M $[^nBu_4N][PF_6]$. Working electrode: gold-coated quartz disk. Scan rate 100 mV/s.)

The gravimetric data associated with the cyclic voltammetry of **1** in acid display a clear increase in the mass (c.a. 30 ng) of the electrode, beginning near the onset of the pseudocatalytic wave at –0.8 V (Figure 4, panel a, blue line). The mass increase continues throughout the reductive sweep, but slows in rate on approach to the switching potential, implying that the precursor material for deposition has been consumed within reaction-diffusion layer. Essentially no mass change is recorded during the portion of the oxidative sweep at potentials less than –0.8 V, confirming that the species responsible for deposition of material was consumed during the first moments of the reductive sweep past –0.8 V. However, during the anodic sweep when passing through the oxidation wave with onset near –0.5 V, the mass precipitously drops, resulting in complete loss of the mass deposited onto the surface during the reductive sweep. These observations implicate deposition of solid cobalt material on the electrode during reductive polarization, and loss of the nascent material during oxidation. In general, this cycle of mass changes is consistent with deposition and anodic stripping[59] of metallic cobalt on the surface.

In our previous report, we showed that the $[BF_2]$-bridged cobaloxime **2** displays related behavior in its voltage-mass profile. In the case of **2**, the cobalt(II/I) couple in the absence of acid is centered at –0.93 V (ΔE_p = 141 mV), and no significant mass change is observable prior to the addition of a proton source (see ESI, Figures S14). When 3 equiv. of $[DMFH]^+[OTf]^-$ are added to a solution of **2**, the quasireversible cobalt(II/I) couple is replaced by a catalytic reductive wave (Figure 4, panel b, black line). For the case of **2**, there are no anodic waves or significant anodic currents over the relevant potential range (0 V to –1.36 V). However, the mass of the electrode increases steadily beyond the threshold of –0.80 V, depositing nearly 50 ng before reaching a plateau region during the anodic sweep. (See Figure 4, panel b, blue line for mass data.) At potentials more positive than –0.75 V, the electrodeposited material is lost from the surface entirely, with the result that no electrodeposited material is on the surface upon return to the initial potential of 0 V.

Comparing the EQCM results for **1** and **2** with $[DMFH]^+$, both systems give rise to electrodeposition of heterogeneous material at nearly identical potentials (ca. –0.80 V; see Figure 5, showing the voltammetric data from Figure 4 plotted in the time domain to demonstrate this similarity). As the potentials showing onset of electrodeposition are virtually identical, similar cobalt-containing precursors can be reasonably implicated to give rise to formation of solid material upon reduction. For complex **2**, we have previously shown that formation of $[Co(MeCN)_6]^{2+}$ leads to electrodeposition and co-generation of the metal-free macrocycle $(dmgBF_2)_2H_2$ (**4**).[47] For complex **1**, the protonated cobaloxime **3** apparently serves as an electrodeposition precursor, likely via $[Co(MeCN)_6]^{2+}$ formed via a minor equilibrium involving exchange of the $dmgH_2$ ligands with acetonitrile. In accord with this proposed pathway, the potential required for electrodeposition of solid material from $[Co(MeCN)_6]^{2+}$ (ca. –0.80 V) is virtually identical to the potential measured here for electrodeposition from acidic solutions of **1** (see ESI, Figure S15).[47]

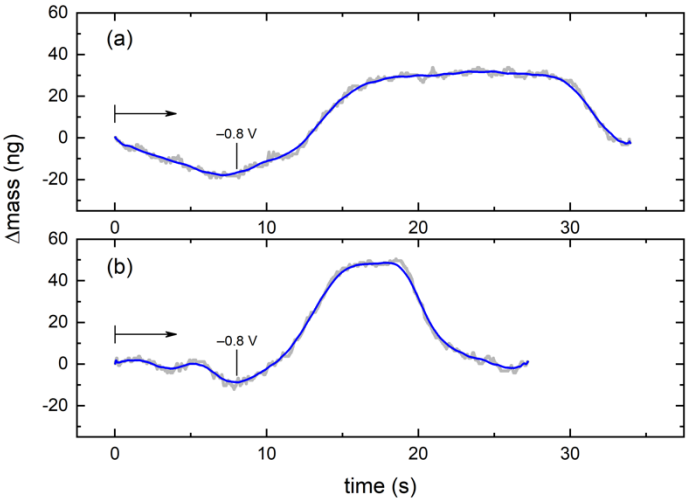

Figure 5. Mass deposition profile of **1** and **2** plotted as a function of time. These mass-time profiles are identical to the mass-voltage data given in Figure 4. (a) 2 mM solution of **1** treated with 3 equiv. $[DMFH]^+[OTf]^-$. Black: Raw mass data, Blue: Smoothed (45-pt adjacent averaged) mass data. (b) 2 mM solution of **2** treated with 3 equiv. $[DMFH]^+[OTf]^-$. Black: Raw mass data, Blue: Smoothed mass data. The time (ca. 8 s in each case) at which –0.8 V is reached is indicated.

In contrast to the similarities in the electrodeposition behavior of **1** and **2** in the presence of $[DMFH]^+$, the processes occurring during anodic cycling that lead to loss of cobalt material from the electrode surface appear different between the two cases. The corrosion of material generated from **2** begins as soon as the potential is swept positive of the deposition onset (–0.80 V), but loss of mass generated from **1** doesn't begin until entering the onset of the broad oxidation near –0.5 V. As this wave has a somewhat asymmetric appearance and resembles an anodic stripping wave, we hypothesize that the current flow corresponds to electrochemical oxidation of nascent Co^0 material on the surface leading to formation of transient $[Co(MeCN)_6]^{2+}$.

Results from previous NMR studies on **2** have shown that c.a. 10% of the starting material decomposes to form a demetallated macrocycle upon treatment with acid,[47] whereas spectroscopic experiments with **1** implicated complete loss of absorptions associated with the parent cobaloxime and formation of **3**. The observed stoichiometry thus suggests that more protons have been consumed in the case of reaction of **1** with 3 equiv. $[DMFH]^+[OTf]^-$, leading to a less acidic solution in the case of experiments with **1** versus **2**. This change in the availability of protons disfavors chemical corrosion,[60] where two protons from a sufficiently acidic source drive *chemical oxidation* of cobalt(0) on the surface to generate soluble cobalt(II) and hydrogen. Instead, secondary material from **1** proceeds through an anodic stripping pathway in which cobalt(0) is *electrochemically oxidized* to release cobalt(II) ions into solution. Presumably, electrodeposited material resulting from the reaction of **2** with strong acid could also be anodically stripped from the electrode surface; however the higher effective acidity of the contacting medium favors chemical corrosion which, at the timescale of this voltammetry, is fast enough to liberate the mass of cobalt material from the surface before the electrode has become sufficiently oxidizing to drive anodic stripping.

Inspection of the gravimetric data plotted as a function of time (Figure 5) highlights the separate appearance of proton-driven chemical corrosion and anodic electrochemical stripping in the behavior of the acid-treated cobaloxime systems. For both **1** (Figure 5, panel a) and **2** (Figure 5, panel b), there is a period of electrode mass increase followed by a "plateau" period during which the electrode mass is essentially constant. At longer timescales, the profiles of **1** and **2** differ in their mass loss behavior, indicative of chemical corrosion taking place with **2**, versus anodic stripping taking place at more positive potentials with **1**.

Calculation of the derivative of the region of mass increase corresponding to electrodeposition in Figure 5 reveals that, in both cases, there is a period of accelerating rate of mass deposition at potentials negative of –0.8 V (see ESI, Figures S20-22). This period is followed by a later period of slowing rate of deposition, which can be readily assigned to depletion of available deposition precursor in each case. Thus, very similar processes give rise to formation of heterogeneous material in each case. Notably, the electrodeposition profile is qualitatively independent of scan rate (see ESI, Figures S21 and S22). Close inspection of the derivative plots (see ESI, Figures S20-S22) reveals a noticeable inflection point in the accelerating deposition rate vs. time plots for all cases, indicating involvement at least two potential-dependent processes in formation of heterogeneous material. As reduction of $[Co(NCMe)_6]^{2+}$ necessarily involves transfer of two electrons, we tentatively postulate that the observed inflection point arises from voltammetric passage through the two separate, but apparently rather closely spaced, $1e^-$ reductions involved in this chemistry.

To summarize, the observation of loss of mass at potentials positive of ca. –0.80 V in experiments with **2** implies that loss of cathodic protection leads to corrosion of Co(0) from electrodes in MeCN solutions containing $[DMFH]^+$. Conversely, under the less acidic conditions in experiments with **1**, anodic stripping of solid Co(0) material on the surface of the electrode is observed at potentials positive of –0.40 V.

Acid-dependent electrochemical studies

As $[Co(MeCN)_6]^{2+}$ is implicated in the behavior of systems containing complexes **1** and **2** with strong acids, we undertook a more detailed investigation of its redox behavior with a series of acids to more directly probe the role of acid strength in governing its electrochemical profile. In the absence of a proton source, $[Co(MeCN)_6]^{2+}$ exhibits a single, mostly irreversible reduction with a cathodic peak potential ($E_{p,c}$) of –1.26 V vs. $Fc^{+/0}$ (Figure 6, panel a, dashed line). On the return anodic scan, a broad oxidative feature is observed with $E_{p,a}$ near +0.3 V; this feature can be assigned as an anodic stripping wave corresponding to oxidation of surface-immobilized Co(0) and formation of free cobalt ions. The addition of 3 equiv. of $[DMFH]^+$ gives rise to enhanced current at the potential of the irreversible reduction, likely a consequence of hydrogen production catalyzed by the nascent electrodeposited cobalt(0) material (Figure 6, panel a, black line). The anodic stripping wave is retained in this experiment, consistent with our prior studies of $[Co(MeCN)_6]^{2+}$ by EQCM.[47]

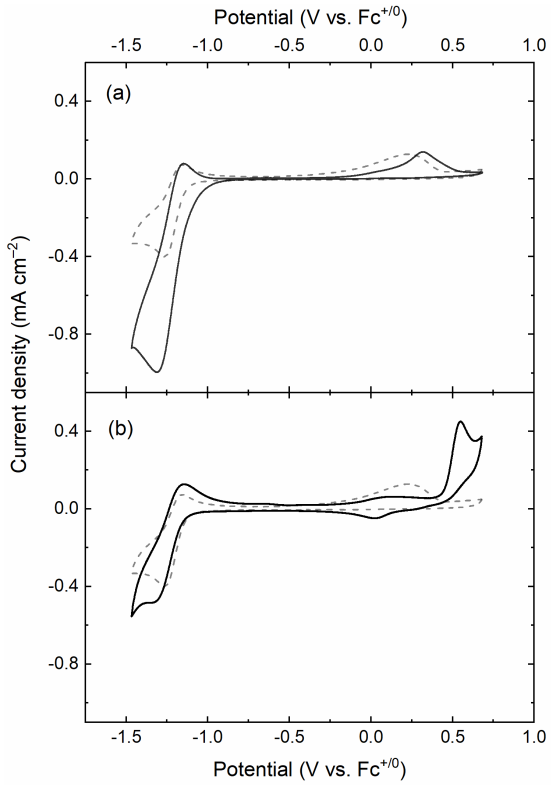

Figure 6. Cyclic voltammograms of the solvento species $[Co(MeCN)_6][BF_4]_2$ from acid addition studies. (a) Dashed Gray: 2 mM $[Co^{2+}]$. Black: 2 mM $[Co^{2+}]$ + 3 equiv. $[DMFH]^+[OTf]^-$. (b) Dashed Gray: 2 mM $[Co^{2+}]$. Black: 2 mM $[Co^{2+}]$ + 3 equiv. $[C_6H_5NH_3]^+[OTf]^-$. (MeCN, 0.1 M $[^nBu_4N][PF_6]$. Working electrode: highly oriented pyrolytic graphite. Scan rate 100 mV/s.

Comparison of these results with those from companion experiments with added $[C_6H_5NH_3]^+$ reveals a role for acid strength in the observed voltammetry. In the presence of anilinium, reductive current flow is enhanced near –1.25 V, but to a lesser extent than that observed for the case of $[DMFH]^+$ (Figure 6, panel b). These observations are consistent with the relative acidities of $[DMFH]^+$ and $[C_6H_5NH_3]^+$ (pK_a values of 6.1 and 10.6),[50,51] since the estimated overpotential for catalytic hydrogen evolution at –1.25 V (the voltage required to produce the solid cobalt metal catalyst) decreases with the acidity of the proton source. Another minor difference appears with anilinium, in that a new anodic process is measured at +0.5 V. This can be reliably assigned as oxidation of aniline,[61] overlapping with the usual anodic stripping wave (Figure 6, panel b).

EQCM results from an experiment examining the behavior of **1** in the presence of anilinium are in accord with these findings, in that formation of heterogeneous material is measured (see ESI, Figure S16). This result supports generation of a sizeable quantity of $[Co(NCMe)_6]^{2+}$ under the chosen conditions. Notably, the potential onset of electrodeposition (–0.8 V) is identical to the other cases investigated here, implying a common precursor complex.[62]

Corrosion rate studies

Having observed these changes in the voltammetry and mass-voltage profiles as a function of acid strength and conditions, we were interested in quantification of the role of acid and molecular precursor structure in corrosion rate. This interest stems from the role of the rate of mass loss in interpretation of data resulting from *ex situ* surface analysis techniques, specifically in regard to studies of molecular catalyst homogeneity. Corrosion is an important phenomenon to consider in such studies, as heterogeneous material formed during electrode polarization may not be stable at open circuit potential or even stable during potential sweeps (as in voltammetry). Thus, studies of corrosion could be useful in informing future studies of molecular electrocatalysis.

As our data suggest the electrodeposited material generated from **1** and **2** in strong acid results from reduction of $[Co(MeCN)_6]^{2+}$ (or a closely related solvento species), $[Co(MeCN)_6][BF_4]_2$ was used as a model compound for these investigations. In the first step of these experiments, linear sweep voltammograms were carried out with polarization from 0 V to –1.5 V in solutions of $[Co(MeCN)_6]^{2+}$ either with or without an added acid (Figure 7). Upon reaching the final potential of –1.5 V, the electrode was returned to the open circuit potential and kept in the electrolyte solution for a further six minutes. The electrode mass was continuously monitored by the EQCM during the potential sweep and during the open circuit period, with the goal of measuring the corrosion rate of the nascent cobalt material on the electrode as a function of the selected electrolyte conditions.

In the absence of acid, the reduction of $[Co(MeCN)_6]^{2+}$ under our conditions results in electrodeposition of 520 ng of heterogeneous material (see Figure 7 for all data). This material is slowly lost from the surface at a rate of –0.4 ng sec^{-1} (Figure 7, black line). Addition of 3 equiv. of $[DMFH]^+$ under otherwise identical conditions results in electrodeposition of slightly less material, 480 ng, consistent with competing electrocatalysis and electrodeposition under these acidic conditions. However, there is a significant increase (5.4x) in corrosion rate to –2.2 ng sec^{-1}. As a result, acid-induced corrosion results in loss of nearly all of the electrodeposited cobalt from the surface within 5 minutes. When $[C_6H_5NH_3]^+$ is substituted for $[DMFH]^+$, the response resembles the case without any acid present, depositing 545 ng of cobalt material and a corrosion rate of –0.67 ng sec^{-1}. The minor enhancement in corrosion rate with $[C_6H_5NH_3]^+$ present (1.6x) suggests that this acid is relatively ineffective in corrosion of cobalt metal.

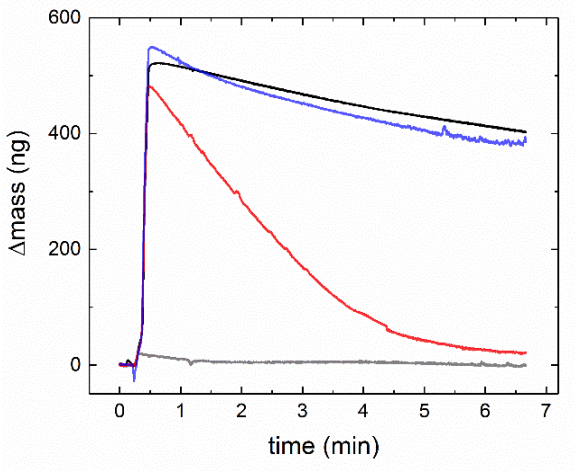

Figure 7. Mass profile of the working electrode surface in experiments done with 2 mM solution of $[Co(MeCN)_6][BF_4]_2$, alone and in the presence of a series of acids. Gray: Background response of the electrode. Black: Response of $[Co^{2+}]$ only. Blue: Response of electrode in solution of $[Co^{2+}]$ with 3 equiv. $[C_6H_5NH_3]^+[OTf]^-$. Red: Response of electrode in solution of $[Co^{2+}]$ with 3 equiv. $[DMFH]^+[OTf]^-$.

With these results in hand, analogous experiments were conducted with **1**. Specifically, an electrolyte solution was prepared containing **1** and 3 equiv. $[DMFH]^+$. Linear sweep voltammetry with simultaneous EQCM monitoring was carried out with polarization from 0 V to –1.7 V, resulting in deposition of 25 ng of nascent cobalt material on the electrode surface (see Figure 8, panel b). Following this potential sweep, the electrode was returned to open circuit. The EQCM reveals an initial period (lasting approximately 5 sec) in which there is essentially no corrosion occurring, as evidenced by a steady mass reading. However, following this steady period, corrosion begins at a rate of approximately –1 ng sec^{-1}. This behavior is consistent with our observations from cyclic voltammetry (Figure 4, panel a), in which acid-induced corrosion is not observed for the transient heterogeneous cobalt material present on the electrode surface. Rather, electrochemical anodic stripping is responsible for rapid loss of cobalt from the electrode surface under those conditions.

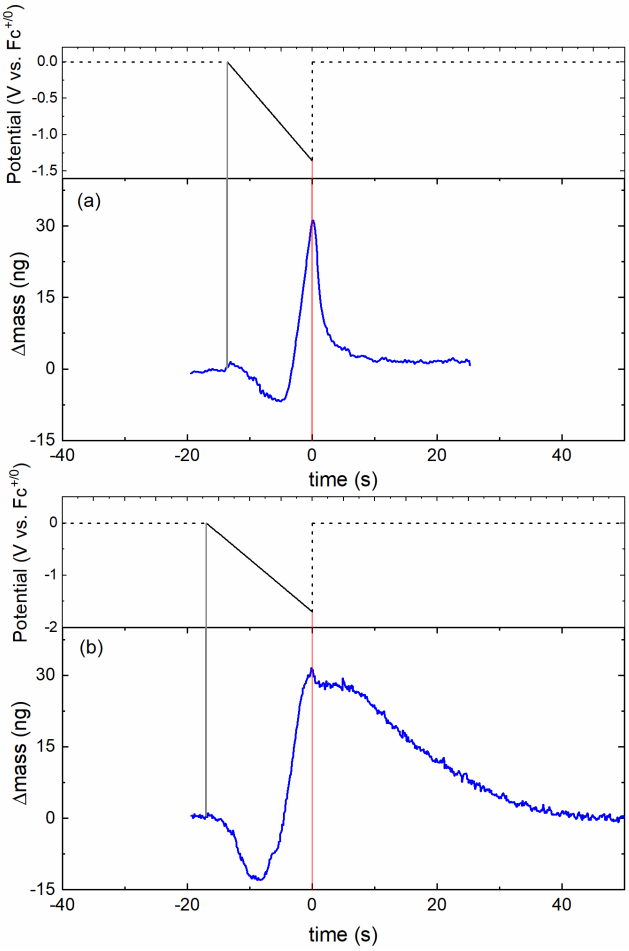

Figure 8. Mass profile of the working electrode surface in experiments done with 2 mM solution of **2** (panel (a)) and **1** (panel (b)) in the presence of $[DMFH]^+$. The upper sub-panels display the polarization as a function of time and the lower sub-panels the mass profile over time. Black: Electrode polarization as a function of time. Blue: Mass profile of the working electrode as a function of time. The grey line denotes the beginning of polarization. The red line shows the time at which polarization ceased and the electrode was allowed to return to open circuit.

Inspection of the anodic stripping wave observed in cyclic voltammetry carried out with **1** (see Figure 4, panel a) supports this interpretation. First, the behavior of the system remains qualitatively identical at all scan rates, with onset of mass deposition near –0.8 V followed by a plateauing region (see ESI, Figure S18 for various scan rates). Slower scan rates increase the time spent at reducing potentials positive of –0.8 V but negative of that required for anodic stripping, ca. –0.4 V. This situation provides a longer time period during which the deposited heterogeneous material may undergo chemical corrosion. Consequently, comparison of the predicted mass lost based on integration of the anodic striping peak with the mass loss directly measured by the EQCM shows that the "efficiency" of anodic stripping (or the relative portion of mass loss attributable to stripping) decreases with slower scan rates (see ESI, Figure S19 for data). Thus, the percentage of the transient heterogeneous material remaining to undergo anodic stripping drops from nearly 100% at 200 mV/s to only

ca. 70% at 50 mV/s. These data reveal the interplay between proton-drive chemical corrosion and anodic electrochemical stripping in the case of **1**, and confirm that both processes can affect the stability of transient heterogeneous materials.

In contrast to the slow initial corrosion rate of –1 ng sec^{-1} measured for **1** (Figure 8), we have previously measured a more rapid rate of –9 ng sec^{-1} for an analogous solution of **2** with 3 equiv. $[DMFH]^+$. In the experiment with **2**, the more rapid corrosion rate results in loss of 32 ng of nascent cobalt material within 7 sec (Figure 8, panel a). This contrasts with the experiment conducted here on **1**, in which a longer time must pass before any appreciable loss of mass from the electrode occurs. Thus, the corrosion rate for cobalt(0) material deposited from a solution of **2** and $[DMFH]^+$ is significantly greater than that observed for an otherwise analogous solution containing **1** (–9 ng sec^{-1} vs. –1 ng sec^{-1}). This difference is attributable to the influence of the unique chemistry of each of the molecular precatalysts/precursors. Specifically, a solution containing **2** and $[DMFH]^+$ contains a greater amount of free $[DMFH]^+$ (on the basis of chemical studies) to drive corrosion behavior than analogous solutions containing **1**. Thus, the observation of enhanced corrosion in the case of **1** vs. **2** is affected, at moderate loadings of acid, by the structural features of the molecular precursors themselves.

3. Conclusions

The EQCM can interrogate and quantify electrodeposition, corrosion, and electrochemical stripping processes that may be involved in the behavior of with molecular catalysts and precatalysts. Here, we have used the EQCM to show that the ligand-centered protonation of cobaloximes can contribute to their electrochemical behavior and catalysis, a situation in which the transient nature of the heterogeneous materials formed under the relevant conditions makes *ex situ* studies challenging. We find that the precatalyst structure and operating conditions play key roles in governing the chemistry that takes place. Capability in revealing the interplay of corrosion and anodic stripping processes of secondary, heterogeneous materials can be highlighted as a specific advantage of the EQCM, as these processes might otherwise evade detection by traditional techniques. Thus, the EQCM can readily assay transient heterogeneous catalyst materials formed even at short times on electrode surfaces, making it useful in molecular electrocatalysis research. Our group is currently pursuing further applications in this area, with an emphasis on improving molecular-level understanding of processes occurring during electrochemical energy conversion.

4. Experimental Section

GENERAL CONSIDERATIONS

All manipulations were carried out in dry, N_2-filled gloveboxes (Vacuum Atmospheres Co., Hawthorne, CA) or under a N_2 atmosphere using standard Schlenk techniques unless otherwise noted. All solvents were of commercial grade and dried over activated alumina using a PPT Glass Contour (Nashua, NH) solvent purification system prior to use, and were stored over molecular sieves. All chemicals were from major commercial suppliers and used after extensive drying. $NOBF_4$ was dried *in vacuo* overnight. CD_3CN was purchased from Cambridge Isotope Laboratories and dried over 3 Å molecular sieves. ^1H NMR spectra were collected on a 400 MHz Bruker spectrometer and referenced to the residual protio-solvent signal.

Synthesis of acids and metal complexes

Protonated dimethylformamide ($[DMFH]^+[OTf]^-$), aniliniumtriflate ($[C_6H_5NH_3]^+[OTf]^-$) and triethylammoniumtriflate ($[Et_3NH]^+[OTf]^-$) were synthesized by the method of Favier and Duñach.[63] $[Co(MeCN)_6][BF_4]_2$, $Co^{II}(dmgH)_2$ and $Co^{II}(dmgBF_2)_2$ were prepared according to procedures in the literature.[49,25]

Spectroscopic instruments and methods

Infrared spectra were recorded on a PerkinElmer Spectrum 100 FTIR spectrometer at room temperature; solution samples were prepared inside a dry N_2-atmosphere glovebox and sealed in 0.1 mm NaCl cells. All measurements were collected in tetrahydrofuran (THF) solution in order to access the spectral regions of interest.

UV-visible spectra were taken with an Ocean Optics Flame Spectrometer. Samples were prepared in a dry, N_2-atmosphere glovebox and dissolved in dry, degassed MeCN in 1-cm path length quartz cuvettes. Spectra were measured in the glovebox using fiber optic feed-throughs.

Electrochemical experiments and methods

Electrochemical experiments were carried out in a N_2-filled glovebox in dry, degassed MeCN. 0.10 M tetra(n-butylammonium) hexafluorophosphate ($[^nBu_4N]^+[PF_6]^-$; Oakwood Chemical, recrystallized from ethanol) served as the supporting electrolyte. Measurements were made with a Gamry Reference 600+ Potentiostat/Galvanostat using a standard three-electrode configuration. The working electrode was the basal plane of highly oriented pyrolytic graphite (HOPG) (GraphiteStore.com, Buffalo Grove, Ill.; surface area: 0.09 cm^2), the counter electrode was a platinum wire (Kurt J. Lesker, Jefferson Hills, PA; 99.99%, 0.5 mm diameter), and a silver wire immersed in electrolyte served as a pseudo-reference electrode (CH Instruments). The reference was separated from the working solution by a Vycor frit (Bioanalytical Systems, Inc.). Ferrocene (Sigma Aldrich; twice-sublimed) was added to an electrolyte solution prior to the beginning of each experiment; the midpoint potential of the

ferrocenium/ferrocene couple (denoted as $Fc^{+/0}$) served as an external standard for comparison of the recorded potentials. Concentrations of analyte for cyclic voltammetry were 2 mM unless otherwise stated.

Piezoelectric gravimetry

Electrochemical quartz crystal microbalance experiments were carried out in a N_2-filled glovebox. Measurements were made with a Gamry eQCM 10M electrochemical quartz crystal microbalance. Solutions were prepared in a static Teflon cell. An AT-cut quartz disk sputtered with gold and having a nominal resonant frequency of 10 MHz was used as the working electrode (Gamry Instruments; electroactive area ca. 0.205 cm^2). The counter electrode was a platinum wire (Kurt J. Lesker, Jefferson Hills, PA; 99.99%, 0.5 mm diameter), and a silver wire immersed in electrolyte served as a pseudo-reference electrode (CH Instruments). The reference was separated from the working solution by a Vycor frit (Bioanalytical Systems, Inc.).

Conflicts of interest

There are no conflicts to declare.

Acknowledgements

The authors thank Dr. Davide Lionetti for numerous helpful discussions, Dr. Justin Douglas and Sarah Neuenswander for assistance with NMR spectroscopy, and Prof. Misha Barybin for use of an IR spectrometer. This work was supported by the US National Science Foundation through award CBET-1605524, and by the University of Kansas. The authors also acknowledge the National Science Foundation and National Institutes of Health (CHE-0320648, S10OD016360, and S10RR024664) for support of NMR instrumentation used in this study.

References

[1]J. Tafel, *Z. Phys. Chem.*, 1905, **50U**, 641.

[2]J. Kiwi and M. Graetzel, *J. Am. Chem. Soc.*, 1979, **101**, 7214.

[3]J. M. McEnaney, J. Chance Crompton, J. F. Callejas, E. J. Popczun, C. G. Read, N. S. Lewis and R. E. Schaak, *ChemComm*, 2014, **50**, 11026.

[4]T. F. Jaramillo, K. P. Jørgensen, J. Bonde, J. H. Nielsen, S. Horch and I. Chorkendorff, *Science*, 2007, **317**, 100.

[5]E. J. Popczun, C. G. Read, C. W. Roske, N. S. Lewis and R. E. Schaak, *Angew. Chem. Int. Ed.*, 2014, **53**, 5427.

[6]D. C. Lacy, C. C. L. McCrory and J. C. Peters, *Inorg. Chem.*, 2014, **53**, 4980.

[7]B. H. Solis, A. G. Maher, T. Honda, D. C. Powers, D. G. Nocera and S. Hammes-Schiffer, *ACS Catal.*, 2014, **4**, 4516.

[8]J. R. McKone, S. C. Marinescu, B. S. Brunschwig, J. R. Winkle and H. B. Gray, *Chem. Sci.*, 2014, **5**, 865.

[9]M. Rakowski Dubois and D. L. Dubois, *Acc. Chem. Res.*, 2009, **42**, 1974.

[10] J.-M. Saveant, *Elements of Molecular and Biomolecular Electrochemistry*, Wiley, Hoboken, NJ, 2006.

[11] A. J. Bard and L. R. Faulkner, *Electrochemical Methods: Fundamentals and Applications*, Wiley, Hoboken, NJ, 2nd edn., 2001.

[12] D. C. Grills, D. E. Polyansky and E. Fujita, *ChemSusChem*, 2017, **10**, 4359-4373.

[13]J. J. Stracke and R. G. Finke, *J. Am. Chem. Soc.*, 2011, **133**, 14872.

[14]N. D. Schley, J. D. Blakemore, N. K. Subbaiyan, C. D. Incarvito, F. D'Souza, R. H. Crabtree and G. W. Brudvig, *J. Am. Chem. Soc.*, 2011, **133**, 10473.

[15]R. H. Crabtree, *Chem. Rev.*, 2015, **115**, 127.

[16]G. M. Whitesides, M. Hackett, R. L. Brainard, J. Lavalleye, A. F. Sowinski, A. N. Izumi, S. S. Moore, D. W. Brown and E. M. Staudt, *Organometallics*, 1985, **4**, 1819.

[17]Y. Lin and R. G. Finke, *Inorg. Chem.*, 1994, **33**, 4891.

[18]J. A. Widegren and R. G. Finke, *J. Mol. Catal. A: Chem.*, 2003, **198**, 317.

[19] B. Lassalle-Kaiser, A. Zitolo, E. Fonda, M. Robert and E. Anxolabéhère-Mallart, *ACS Energy Letters*, 2017, **2**, 2545-2551.

[20]J. Hawecker, J. Lehn and R. Ziessel, *Nouv. J. Chim.*, 1983, **7,** 271.

[21]P. Connolly and J. H. Espenson, *Inorg. Chem.*, 1986, **25**, 2684.

[22]G. N. Schrauzer, *Acc. Chem. Res.*, 1968, **1**, 97.

[23]G. Costa, G. Mestroni and E. de Savorgnani, *Inorg. Chim. Acta*, 1969, **3**, 323.

[24]G. N. Schrauzer, *Angew. Chem. Int. Ed.*, 1976, **15**, 417.

[25]B. S. Tovrog, D. J. Kitko and R. S. Drago, *J. Am. Chem. Soc.*, **1976**, *98*, 5144.

[26]K. A. Lance, K. A. Goldsby and D. H. Busch, *Inorg. Chem.*, 1990, **29**, 4537.

[27]J. Willkomm, N. M. Muresan and E. Reisner, *Chem. Sci.*, 2015, **6**, 2727.

[28]S. M. Laga, J. D. Blakemore, L. M. Henling, B. S. Brunschwig and H. B. Gray, *Inorg. Chem.*, 2014, **53**, 12668.

[29]L. M. Utschig, S. C. Silver, K. L. Mulfort and D. M. Tiede, *J. Am. Chem. Soc.*, 2011, **133**, 16334.

[30]A. Krawicz, J. Yang, E. Anzenberg, J. Yano, I. D. Sharp and G. F. Moore, *J. Am. Chem. Soc.*, 2013, **135**, 11861.

[31]G. F. Moore and I. D. Sharp, *J. Phys. Chem. Lett.*, 2013, **4**, 568.

[32]X. Hu, B. S. Brunschwig and J. C. Peters, *J. Am. Chem. Soc.*, 2007, **129**, 8988.

[33]M. Razavet, V. Artero and M. Fontecave, *Inorg. Chem.*, 2005, **44**, 4786.

[34]P. A. Jacques, V. Artero, J. Pecaut and M. Fontecave, *Proc. Nat. Acad. Sci. U.S.A.*, 2009, **106**, 20627.

[35]J. T. Muckerman and E. Fujita, *Chem. Commun.*, 2011, **47**, 12456.

[36]J. L. Dempsey, J. R. Winkler and H. B. Gray, *J. Am. Chem. Soc.*, 2010, **132**, 16774.

[37]G. N. Schrauzer and R. J. Holland, *J. Am. Chem. Soc.*, 1971, **93**, 1505.

[38]A. Bhattacharjee, M. Chavarot-Kerlidou, E. S. Andreiadis, M. Fontecave, M. J. Field and V. Artero, *Inorg. Chem.*, 2012, **51**, 7087.

[39]D. C. Lacy, G. M. Roberts and J. C. Peters, *J. Am. Chem. Soc.*, 2015, **137**, 4860.

[40]T. M. McCormick, Z. Han, D. J. Weinberg, W. W. Brennessel, P . L. Holland and R. Eisenberg, *Inorg. Chem.*, 2011, **50**, 10660.

[41]E. S. Rountree, D. J. Martin, B. D. McCarthy and J. L. Dempsey, *ACS Catal.*, 2016, **6**, 3326.

[42]S. Cobo, J. Heidkamp, P. A. Jacques, J. Fize, V. Fourmond, L. Guetaz, B. Jousselme, V. Ivanova, H. Dau, S. Palacin, M. Fontecave and V. Artero, *Nat. Mater.*, 2012, **11**, 802.

[43]C. C. L. McCrory, C. Uyeda and J. C. Peters, *J. Am. Chem. Soc.*, 2012, **134**, 3164.

[44]N. Kaeffer, A. Morozan, J. Fize, E. Martinez, L. Guetaz and V. Artero, *ACS Catal.*, 2016, **6**, 3727.

[45]E. Anxolabehere-Mallart, C. Costentin, M. Fournier, S. Nowak, M. Robert and J.-M. Saveant, *J. Am. Chem. Soc.*, 2012, **134**, 6104.

[46]E. Anxolabehere-Mallart, C. Costentin, M. Fournier and M. Robert, *J. Phys. Chem. C*, 2014, **118**, 13377.

[47]D. J. Sconyers and J. D. Blakemore, *ChemComm*, 2017, **53**, 7286.

[48] N. D. Schley, J. D. Blakemore, N. K. Subbaiyan, C. D. Incarvito, F. D'Souza, R. H. Crabtree and G. W. Brudvig, *J. Am. Chem. Soc.*, 2011, **133**, 10473-10481.

[49]G. N. Schrauzer, *Inorg. Synth.*, 1968, **11**, 61.

[50] J. T. Muckerman, J. H. Skone, M. Ning and Y. Wasada-Tsutsui, *Biochim. Biophys. Acta, Bioenerg.* 2013, **8**, 882.

[51]A. M. Appel and M. L. Helm, *ACS Catal.*, 2013, **4**, 630.

[52]J. O. Alben, S. S. Choi, A. D. Adler and W. S. Caughey, *Ann. N.Y. Acad. Sci.*, 1973, **206**, 278.

[53]R. A. Heintz, J. A. Smith, P. S. Szalay, A. Weisgerber and K. R. Dunbar, *Inorg. Synth.*, 2002, **33**, 75.

[54]K. Burger, I. Ruff and F. Ruff, *J. Inorg. Nucl. Chem.*, 1965, **27**, 179.

[55]C. L. Perrin and J. B. Nielson, *J. Annu. Rev. Phys. Chem.*, 1997, **48**, 511.

[56]B. H. Solis, Y. Yu, S. Hammes-Schiffer, *Inorg. Chem.*, 2013, **52**, 6994.

[57]D. A. Buttry and M. D. Ward, *Chem. Rev.*, 1992, **92**, 1355.

[58]G. Sauerbrey, *Z. Phys.*, 1959, **155,** 206.

[59]M. Pourbaix, *Lectures on Electrochemical Corrosion*, Plenum Press, 1973.

[60] M. Pourbaix, *Atlas of Electrochemical Equilibria in Aqueous Solutions*, Pergamon Press, 1966.

[61]A. Watanabe, K. Mori, M. Mikuni, Y. Nakamura and M. Matsuda, *Macromolecules*, 1989, **22**, 3323.

[62] A similar experiment carried out with **1** in the presence of Et_3NH^+ does not show formation of heterogeneous material at –0.8 V, suggesting that this significantly weaker acid is not capable of protonation of **1** (see ESI, Figure S17). However, a minor mass increase of the electrode is detected at the Co(II/I) potential, suggesting that another decomposition mechanism may be operative that requires initial reduction of cobalt. See references 45 and 46 for discussion of such pathways for related oxime complexes.

[63]I. Favier and E. Duñach, *Tetrahedron Lett.*, 2004, **45**, 3393.